Rotating Membrane Inclusions Crystallize Through Hydrodynamic and Steric Interactions

Naomi Oppenheimer,[1,*] David B. Stein,[1] and Michael J. Shelley[1,2,†]
[1]Center for Computational Biology, Flatiron Institute, New York, New York 10010, USA
[2]Courant Institute, New York University, New York, New York 10012, USA

(Received 12 March 2019; published 3 October 2019)

We show that rotating membrane inclusions can crystallize due to combined hydrodynamic and steric interactions. Alone, steric repulsion of unconfined particles, even with thermal fluctuations, does not lead to crystallization, nor do rotational hydrodynamic interactions which allow only a marginally stable lattice. Hydrodynamic interactions enable particles to explore states inaccessible to a nonrotational system, yet, unlike Brownian motion, Hamiltonian conservation confines the ensemble which, when combined with steric interactions, anneals into a stable crystal state.

DOI: 10.1103/PhysRevLett.123.148101

Biological membranes serve as barriers between the cell and the outer environment, but unlike most barriers, biomembranes are fluid [1]. There is immense significance to their fluidity as it enables cell signaling, cell division, and more [2]. Moreover, the membrane is not a strictly two-dimensional (2D) fluid. At large distances the fluids outside and inside the cell influence the flow in the plane of the membrane. Thus, the membrane has mixed dimensionality, transitioning between 2D behavior at small distances to three-dimensional (3D) behavior at large distances. The typical distance where this transition occurs is $\lambda = \eta_{2D}/(2\eta_{3D})$ [3], where η_{2D} is the 2D viscosity of the membrane and η_{3D} is the 3D viscosity of the outer fluid. For biological membranes $\lambda \sim 1\ \mu$m, much larger than typical protein sizes ($\sim$10 nm). Two-dimensional fluid films are also ubiquitous in science and in industry [4].

In this Letter, we focus on rotating inclusions in a membrane. An important biological example is ATP synthase, a transmembrane protein pivotal in the energetic balance of the cell [see Fig. 1(a) for a cartoon of the system] [5–12]. Ensembles of such *rotor proteins* are self-driven active matter [13–15]. Since no external torque acts upon the protein its induced flow resembles a torque dipole to leading order [6]. Recently studied synthetic examples of 2D rotor systems have been collections of externally driven particles, such as magnetic colloids at an interface or surface, rotated by an outer magnetic field [15]. For microscopic rotors, inertia is negligible. For larger systems, where inertia cannot be neglected, crystallization can also occur, but from a mechanism reliant upon the Magnus effect (an inertial lift force) and hydrodynamically mediated attraction [16,17]. Both effects are absent in the viscous limit we consider.

By studying infinite systems of model rotor proteins, it was suggested by Lenz *et al.* [5,6] that a hexagonal lattice is a marginally stable state of the system. For finite systems we show that adding steric interactions leads to a lattice state even when starting from random initial conditions. We term these combined hydrodynamic and steric interactions as "hydrosteric." Figures 1(b)–1(d) show the central result of this work—snapshots of three different simulations of rotor protein assemblies, interacting via different combinations of short-ranged repulsion and rotation: panel (b) (marked ⊙), only rotational hydrodynamic interactions; panel (c) (marked ✳), only repulsive interactions; and panel (d) (marked ⊛), both rotational and repulsive interactions. The insets show the structure factor of each system, given

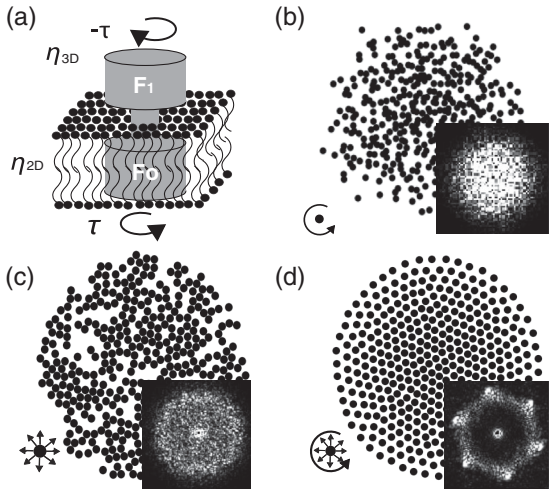

FIG. 1. (a) A membrane protein represented as two counter-rotating disks, one in the membrane, the other in the outer fluid, with torque strengths τ and $-\tau$, respectively. (b)–(d) Snapshots of three simulations, with the same initial conditions and taken at the same time, of (b) rotor proteins with only rotation and no repulsion, (c) only repulsion and no rotation, and (d) both rotation and repulsion. The inset of each figure is the structure factor, showing hexatic ordering for (d) but no distinct ordered structure for (b) and (c). Systems (c) and (d) are at an area fraction of 0.53.

by $S(\mathbf{q}) = 1/N \sum_{i,j} e^{-i\mathbf{q}\cdot(\mathbf{r}_i - \mathbf{r}_j)}$, where N is the number of particles in the ensemble [18]. The six distinct peaks in the structure factor of system ❀ indicate the presence of global hexagonal order, vs no distinct ordered structure in $S(\mathbf{q})$ of systems ☉ and ✻ (see Supplemental Material for a video [19]).

Rotational interactions can resemble thermal fluctuations, allowing the system to sample configurations in phase space. However, in unbounded systems, thermal forces drive particles apart, while rotational interactions do not. Further, a bounded or periodic system of hard disks starts to order only at $\phi \sim 0.7$ [20,21]. We observe hydrosteric crystallization at much lower area fractions, $\phi \sim 0.45$ (see Fig. 1 and Supplemental Material). In what follows we present simulations of rotor proteins, but the essential results are general and should apply to any 2D rotor systems with the same symmetries.

The hydrodynamic model and its properties.—We start by describing a driven membrane rotor, modeled as a single disk of radius a rotating due to an external torque τ, in a flat membrane at $z = 0$ whose 2D velocity is $\mathbf{v}$. We assume membrane incompressibility ($\nabla \cdot \mathbf{v} = 0$), and negligible inertia (small Reynolds number). Under these assumptions, momentum conservation in the membrane reads

$$\eta_{2D}\nabla^2\mathbf{v} + \eta_{3D}\left(\frac{\partial \mathbf{u}}{\partial z}\right)_{z=0} + \tau\nabla^{\perp}\delta(\mathbf{r}) = 0, \qquad (1)$$

where $\mathbf{u}$ is the $\mathbf{r} = (x, y)$ components of the 3D flow in the outer fluids, and $\nabla^{\perp} = (-\partial/\partial y, \partial/\partial x)$. The second term is the jump in shear stress from the outer fluids, and the third is the force due to a point torque. There is no pressure contribution for purely rotational motion, or a superposition of such flows. The outer fluids obey the 3D Stokes equations with the boundary condition $\mathbf{u}^{\pm}|_{z=0} = \mathbf{v}$. The 2D stream function Ψ of the velocity $\mathbf{v}$ can be computed using a 2D Fourier transform [$\tilde{F}(\mathbf{q}) = \int\int F(\mathbf{r}) e^{i\mathbf{q}\cdot\mathbf{r}} d^2r$], giving

$$\tilde{v}(q) = \frac{\tau}{\eta_{2D}}\nabla^{\perp}\tilde{\Psi}; \qquad \tilde{\Psi} = \frac{1}{q(q + \lambda^{-1})}. \qquad (2)$$

In real space $\Psi(\mathbf{r}) = 1/4[H_0(r/\lambda) - Y_0(r/\lambda)]$, where H_0 and Y_0 denote the order zero Struve function and Bessel function of the second kind, respectively.

For a rotor protein, a second counterrotating disk is placed a distance l away in the outer fluid, such that the total torque on the protein is zero [see Fig. 1(a)]. A similar derivation assuming $r \gg l$ (see Supplemental Material [19] and Ref. [5]), gives

$$\mathbf{v}(\mathbf{r}) = \Gamma\nabla^{\perp}\Psi,$$
$$\Psi(\mathbf{r}) = \frac{1}{2\pi}\left\{\frac{\lambda}{r} + \frac{\pi}{2}\left[Y_0\left(\frac{r}{\lambda}\right) - H_0\left(\frac{r}{\lambda}\right)\right]\right\}, \qquad (3)$$

where $\Gamma = 2\tau l/\eta_{2D}\lambda$. For small distances $r \ll \lambda$, the stream function satisfies $\Psi \sim 1/r$. Therefore, $v \sim \nabla^{\perp}\Psi \sim 1/r^2$. Qualitatively, this can be understood as follows: in a 2D fluid, a Stokeslet [the flow due to a point force $\delta(\mathbf{r})$] scales as $\log r$; a rotlet [the flow due to a point torque $\nabla^{\perp}\delta(\mathbf{r})$] thus scales as $v \sim 1/r$. A torque dipole produces another derivative, leading to $v \sim 1/r^2$. In the opposite limit, $r \gg \lambda$, the 3D fluid dominates. A Stokeslet scales as $1/r$. The flow due to a rotating protein should scale as $1/r^3$, but this term cancels due to symmetry at the $z = 0$ plane, and we have $v \sim 1/r^4$.

For more than one rotor protein, the stream function generalizes to the Hamiltonian $\mathcal{H} = \sum_{i\neq j}\Gamma_i\Gamma_j\Psi(|r_i - r_j|)$, where $\Gamma_i = 2\tau_i l/\eta_{2D}\lambda$ is the strength of the ith torque dipole. The velocity is given by $\mathbf{v}_i = (1/\Gamma_i)\nabla_i^{\perp}\mathcal{H}$ [22]. Note that $\mathcal{H}$ is a Hamiltonian in the 2D coordinates, x and y, and so phase space corresponds to the positions of the rotors. From Noether's theorem [23], symmetries of the Hamiltonian correspond to conservation laws. In our case there is conservation of the Hamiltonian itself, and of the first and second moments (from time, translational, and rotational invariance, respectively).

We take all the "circulations" Γ_i, to be equal, $\Gamma_i = \Gamma$ [24]. Conservation of the second moment then simplifies to $\mu_2 = \sum_{i,j}|r_i - r_j|^2 = \text{const}$. As a result of this invariance the distance between rotors cannot diverge to infinity, and by invariance of $\mathcal{H}$ the distance cannot collapse to zero. In general, rotor ensembles stay bounded in an area not much different from their initial area. A crude upper bound for the radius of the rotating system can be derived as follows. For a random initial condition, the second moment is proportional to the initial area and the number of particles squared, i.e., $\mu_2 \sim r_0^2N^2$. The maximal radius is bounded by a configuration in which all particles but one are at the origin. The remaining particle will have the maximal possible distance from the origin, $r_{\max} \leq \sqrt{\mu_2/N} \propto r_0\sqrt{N}$. This bound can be refined by incorporating the conservation of $\mathcal{H}$, see Supplemental Material [19].

Surprisingly, the dynamics of this overdamped system is similar to that of point singularities in 2D such as the ideal vortices of a 2D Euler fluid, or those of the quasigeostrophic equations which arise in modeling atmospheric flows [25,26]. In all such systems two singularities will orbit around each other, and for four or more the system becomes nonintegrable leading to chaotic dynamics [27]. Indeed, the near-field interactions for rotor proteins are the same as for quasigeostrophic vortices.

In what follows, we consider two aspects of membrane inclusions that are not captured by pure hydrodynamic interactions. First, membrane inclusions are physical objects of a finite size with possible interactions with each other. Second, due to their small size (~10 nm) thermal noise may influence their dynamics. We show that adding any type of repulsion between the rotors can result in the formation of crystals; sufficiently high temperature can destroy that order.

Repulsive interactions drive crystallization.—An infinite hexagonal array of rotor inclusions with only hydrodynamic

interactions (system ⊙) is in a steady state for any lattice scale d [5]. Because of its Hamiltonian structure, this array is at most neutrally stable: a disordered array will not crystallize (see Supplemental Material). Repulsive interactions (system ❋) add stability to this fixed point. A linear perturbation $\delta r(t)$ on a single rotor must have the form $d\delta\mathbf{r}/dt = -\alpha\delta\mathbf{r}_\perp - \beta\delta\mathbf{r}$, where α (β) arises from rotational (repulsive) interactions. The eigenvalues of this system are $\lambda = \pm i\alpha - \beta$; the additional negative component is necessary for linear stability of the hexagonal configuration. Simple symmetry arguments show that an infinite or confined system with long-ranged repulsive interactions must form a hexagonal lattice, known as a Wigner crystal [28].

However, this is not the case for a finite system with only short-ranged repulsive interactions; see Fig. 1(c). Surprisingly, we find that crystallization still occurs in such a system when rotation is induced. We examine the dynamics of a finite, unconfined system of rotor proteins with short-ranged repulsion with an interaction distance r_s, using either soft, harmoniclike, repulsion $U = U_0(r - r_s)^2$, up to an interparticle distance of r_s, and zero otherwise, or exponential (e.g., electrostatically screened interactions) $U = U_0 e^{-r/r_s}$.

Evolving the system from random initial conditions, we discovered that rotation promotes rapid organization into crystals, even when repulsion alone is not sufficient to generate crystallization; see Figs. 1(c) vs 1(d). In system ❋, a particle moves until it no longer feels its neighbors. At low concentrations, the system settles in a disordered state. Adding rotation to the particles, system ⊛, stirs and reshuffles them, until a steady state configuration is reached where particles are nearly equispaced.

Increased rotor activity yields faster ordering.—To measure order we examine the structure factor $S(\mathbf{q})$ and the two-dimensional bond-orientational order parameter $\Psi_6^j = (1/n_j)\sum_i e^{i6\theta_{ij}}$. Ψ_6^j measures the orientation and degree of hexagonal order around particle j [29], the sum taken over the nearest neighbors of particle j as found from Delaunay triangulation [30], n_j is the number of nearest neighbors, and θ_{ij} is the angle between the bond connecting particles i and j and the x axis (an arbitrary reference). Let $\langle\cdot\rangle$ define averages over all ensemble particles. We define the average local and global order parameters as $\langle|\Psi_6|\rangle$ and $|\langle\Psi_6\rangle|$, respectively. $|\langle\Psi_6\rangle|$ is nearly zero for all initial random configurations, and is one for a perfect infinite hexagonal lattice. Purely repulsive interactions lead to a slight increase in the order parameter (see Fig. 2), but do not generate completely ordered arrays. Increasing the circulation Γ increases order in the system, saturating $\langle|\Psi_6|\rangle$ at a value of ~0.9. Repulsive interactions promote crystallization but are unnecessary for maintaining order: once the system has reached the state shown in Fig. 1(d), turning off repulsive interactions does not destroy the order.

Estimating the lattice rotation rate.—Once formed, the crystals are not stationary, but rotate around their center of mass with an angular velocity $\Omega(r)$. Figure 3 shows the angular velocity as a function of radius for a finite system of particles interacting via Eq. (3) and exponential repulsion. We note two things about the angular velocity. First, it decreases with time [Fig. 3(a)] due to the exponential repulsion. Second, increasing the number of rotors (with fixed initial area) results in an increase in Ω, see Fig. 3(b). To explain these features, we construct a simplified model based on two observations from Figs. 1(d) and 3(a): (1) the lattice rotates as a nearly rigid body, and (2) it forms a nearly perfect lattice. We hence assume rigid body rotation of a lattice with a spacing d and angular velocity $\bar{\Omega}$. With these simplifications, the velocity in an infinite system must be zero from symmetry. To see this, consider the central particle in Fig. 3(c) (marked with a cross). Each two opposing particles surrounding it will create opposite flows resulting in zero net velocity. For an infinite system all particles are identical; therefore, the velocity of each particle is zero. Thus, for a finite system of size R, the perimeter dictates the angular velocity of the lattice, namely, the number of proteins on the edge n_r and the distance between them d, see Fig. 3(c). For $R \ll \lambda$, the

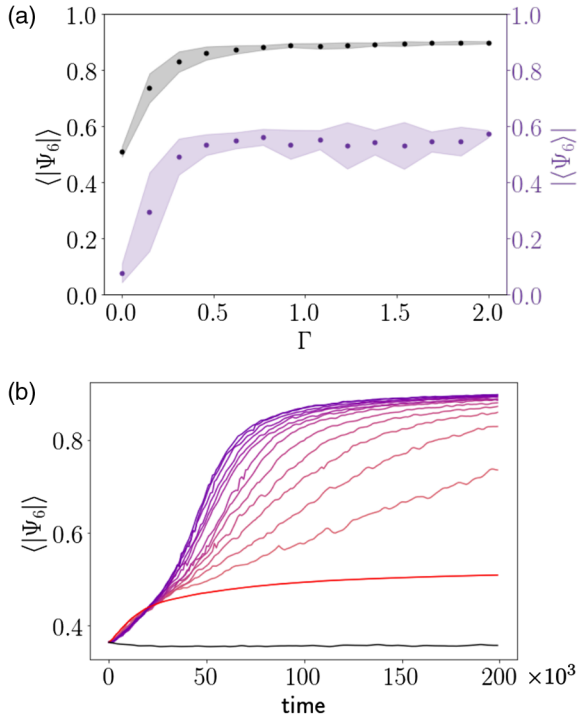

FIG. 2. (a) The average local $\langle|\Psi_6|\rangle$ (black) and global $|\langle\Psi_6\rangle|$ (purple) bond order parameters as a function of circulation Γ, calculated after 2×10^5 time steps for ensemble sizes much smaller than λ. Each point corresponds to an average over 14 random initial configurations in a system of 400 motors with soft-core repulsion, with a final area fraction of ~0.8. Shaded regions are the standard deviation. (b) The local order parameter as a function of time. The hue increases with circulation. The black curve corresponds to the case of no repulsion, the red curve corresponds to the case of no rotation.

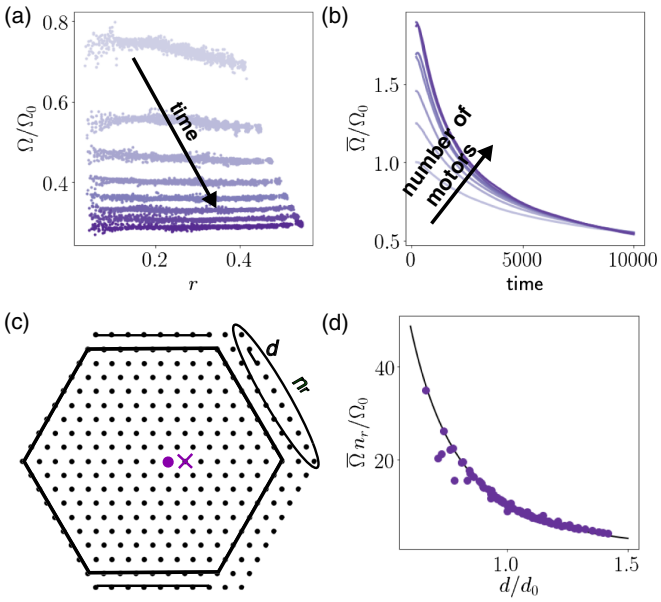

FIG. 3. (a) Angular velocity Ω as a function of radius, increased hue corresponds to progression in time. Density decreases with time, resulting in lower angular velocity. At long times the lattice rotates as a nearly rigid body. (b) The increase in hue corresponds to increasing the number of rotors, from 100 to 1200. (c) Assuming rigid body rotation and a perfect, finite, hexagonal lattice, whose center is marked with a cross symbol, the angular velocity of the point marked with a dot is equal to that of the entire crystal. From symmetry, any motor in the gray hexagon or on the black lines will not contribute. (d) Scaling the average angular velocity according to Eq. (4), all results fall on a single curve. The angular velocity in all subfigures is normalized by $\Omega_0 = \Omega(t = 0)$ for 200 rotors.

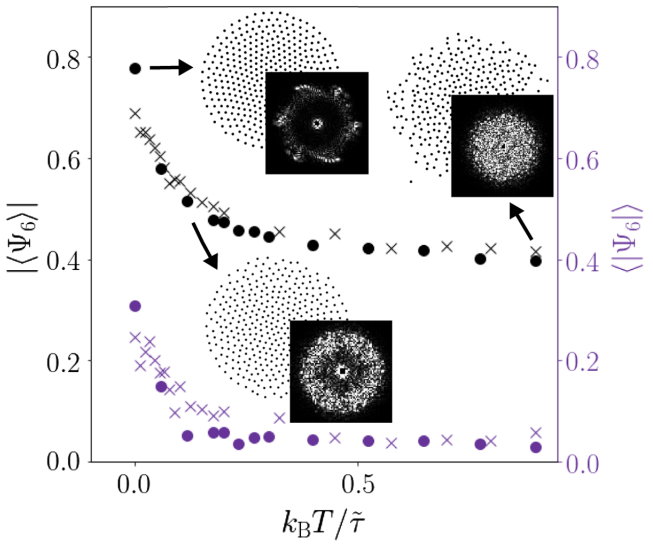

FIG. 4. Thermal effect on the global (purple) and local (black) bond order parameters in a system of 200 (crosses) and 400 (circles) particles. Results are given for an average over nine random initial configurations. Snapshots of the system at three different temperatures, at the same time, are shown, along with their corresponding structure factors.

velocity of the kth protein, in complex notation $z = x + iy$, is $dz_k/dt = i\sum_j [(z_k - z_j)/|z_k - z_j|^3]$, with distance normalized by λ, and time by $2\pi\lambda^2/\Gamma$. Assuming $\Omega = \text{const}$, we can calculate it by considering any one protein, e.g., the particle marked with a disk in Fig. 3(c), with $z_k = -De^{i\Omega t}$, where $D = d/\lambda$. All rows except the four edges cancel, and as $n_r \to \infty$ this gives

$$\Omega \xrightarrow{N\to\infty} \frac{4}{D^3}\sum_{j=0}^{n_r}\frac{\cos(\pi n/3n_r)}{n_r^2} = \frac{6\sqrt{3}}{\pi D^3 n_r}. \tag{4}$$

After scaling Ω at different times and for different system sizes according to Eq. (4), all results fall on a single curve; see Fig. 3(d). In the opposite limit ($d \gg \lambda$) we get $\Omega \propto 1/(D^3 n_r^3)$ (see Supplemental Material).

Effect of thermal noise.—Proteins are small (~10 nm) and prone to thermal forces. Thermal fluctuations must be added carefully when hydrodynamic interactions are included, as the thermal motion of one protein effects others via the fluid. To account for this, we use the positive definite analog of the Rotne-Prager mobility tensor for a membrane, given in Ref. [31]. Figure 4 presents the results of increasing temperature on $\langle|\Psi_6|\rangle$ and $|\langle\Psi_6\rangle|$ for two systems (with 200 and 400 rotor proteins). At low temperatures the systems are ordered, transitioning to disorder at about $k_BT/\tilde{\tau} \sim 0.3$, where $\tilde{\tau} = \eta_{2D}\Gamma$ is the torque-dipole strength acting on a rotor.

To estimate the biologically relevant regime, we take the Péclet number to be $\text{Pe} = va/D$, where v is the hydrodynamic advective velocity of Eq. (3) summed over all particles in the ensemble, and D is the diffusion coefficient of a rotor protein. Using measurements in the literature for membrane viscosity (~1 Pa s [32]), the protein rotation rate (~10^2–10^3 Hz [7,11,33]) and size (~10 nm [7]), we estimate the Péclet number for ATP synthase to be $\text{Pe} \sim 2$. In our simulations, this corresponds to a normalized energy of $k_BT/\tilde{\tau} \sim 0.1$, below the transition point. Thus, biological systems should be in a relatively ordered state, but thermal noise is not negligible (see the middle snapshot in Fig. 4). This estimate does not incorporate steric interactions which we expect to further stabilize the system. Experimental evidence exists of lattice formation of ATP synthases in lipid vesicles and in the mitochondria [8,12,34]. However, both dimerization [8,34] and curvature [12,35] can play significant roles in those systems, which are beyond the scope of this work.

Discussion.—A system of rotor inclusions self-organizes into a hexagonal lattice through hydrosteric interactions. At low rotor protein concentrations, with only repulsion, the system (✻) is quenched in a disordered state. Adding rotation (❀), shuffles the positions of the particles through their hydrodynamic interactions, driving them to an ordered state. Similarly to thermal agitation, activity allows the

system to explore phase space, but unlike temperature, the two conserved quantities, the Hamiltonian $\mathcal{H}$ and the second moment of the distribution μ_2, restrict the domain of accessible states. The rotational system is thus self-confining, whereas with temperature, an initial configuration will spread to infinity as $\sqrt{t}$.

We thank M-Y. Ben Zion, E. Lushi, D. Saintillan, and F. Balboa for useful discussions. M. J. S. thanks the NSF for support through Grants No. DMR-1420073 (NYUMRSEC), No. DMS-1463962, and No. DMS-1620331.

*naomiop@gmail.com
†mshelley@flatironinstitute.org

[1] S. J. Singer and G. L. Nicolson, Science **175**, 720 (1972).
[2] R. Phillips, *Physical Biology of the Cell* (Garland Science, New York, 2013).
[3] P. G. Saffman and M. Delbrück, Proc. Natl. Acad. Sci. U.S.A. **72**, 3111 (1975).
[4] C. Isenberg, *The Science of Soap Films and Soap Bubbles* (Dover Publications, New York, 1992), p. 188.
[5] P. Lenz, J.-F. Joanny, F. Jülicher, and J. Prost, Phys. Rev. Lett. **91**, 108104 (2003).
[6] P. Lenz, J. F. Joanny, F. Jülicher, and J. Prost, Eur. Phys. J. E **13**, 379 (2004).
[7] H. Ueno, T. Suzuki, K. Kinosita, and M. Yoshida, Proc. Natl. Acad. Sci. U.S.A. **102**, 1333 (2005).
[8] N. Buzhynskyy, P. Sens, V. Prima, J. N. Sturgis, and S. Scheuring, Biophys. J. **93**, 2870 (2007).
[9] D. Okuno, R. Iino, and H. Noji, J. Biochem **149**, 655 (2011).
[10] K. M. Davies, C. Anselmi, I. Wittig, J. D. Faraldo-Gómez, and W. Kühlbrandt, Proc. Natl. Acad. Sci. U.S.A. **109**, 13602 (2012).
[11] J. L. Martin, R. Ishmukhametov, T. Hornung, Z. Ahmad, and W. D. Frasch, Proc. Natl. Acad. Sci. U.S.A. **111**, 3715 (2014).
[12] C. Jiko, K. M. Davies, K. Shinzawa-Itoh, K. Tani, S. Maeda, D. J. Mills, T. Tsukihara, Y. Fujiyoshi, W. Kühlbrandt, and C. Gerle, eLife, https://doi.org/10.7554/eLife.06119 (2015).
[13] N. H. P. Nguyen, D. Klotsa, M. Engel, and S. C. Glotzer, Phys. Rev. Lett. **112**, 075701 (2014).
[14] K. Yeo, E. Lushi, and P. M. Vlahovska, Phys. Rev. Lett. **114**, 188301 (2015).
[15] V. Soni, E. Bililign, S. Magkiriadou, S. Sacanna, D. Bartolo, M. J. Shelley, and W. T. M. Irvine, Nat. Phys., https://doi.org/10.1038/s41567-019-0603-8 (2019).
[16] Y. Goto and H. Tanaka, Nat. Commun. **6**, 5994 (2015).
[17] B. A. Grzybowski, H. A. Stone, and G. M. Whitesides, Nature (London) **405**, 1033 (2000).
[18] P. M. Chaikin and T. C. Lubensky, *Principles of Condensed Matter Physics* (Cambridge University Press, Cambridge, England, 1995).
[19] See Supplemental Material at http://link.aps.org/supplemental/10.1103/PhysRevLett.123.148101 for the derivation of the stream function of a rotor protein; a detailed calculation of the angular velocity; an upper and lower bounds for an ensemble of proteins; results for an exponential repulsion; phase diagram of the order parameter when changing repulsion strength and area fraction; and, a movie of the dynamics of the three different systems.
[20] M. Engel, J. A. Anderson, S. C. Glotzer, M. Isobe, E. P. Bernard, and W. Krauth, Phys. Rev. E **87**, 042134 (2013).
[21] S. C. Kapfer and W. Krauth, Phys. Rev. Lett. **114**, 035702 (2015).
[22] E. Lushi and P. M. Vlahovska, J. Nonlinear Sci. **25**, 1111 (2015).
[23] E. Noether, Transport Theor. Stat. **1**, 186 (1971).
[24] For ATP synthase, angular velocity of the proteins is a function of proton concentration. Since protons are 7 orders of magnitude smaller than the proteins, we can assume that proton concentration equilibrates on a much faster timescale.
[25] G. Falkovich, J. Phys. A **42**, 123001 (2009).
[26] G. Conti and G. Badin, Fluids **2**, 50 (2017).
[27] H. Aref and N. Pomphrey, Proc. R. Soc. A **380**, 359 (1982).
[28] E. Wigner, Phys. Rev. **46**, 1002 (1934).
[29] D. R. Nelson, *Defects and Geometry in Condensed Matter Physics* (Cambridge University Press, Cambridge, England, 2002).
[30] P. B. Delaunay, Bull. Acad. Sci. USSR **7**, 793 (1934).
[31] Y. Sokolov and H. Diamant, J. Chem. Phys. **149**, 034901 (2018).
[32] Y. Wu, M. Štefl, A. Olzyńska, M. Hof, G. Yahioglu, P. Yip, D. R Casey, O. Ces, J. Humpolíčková, and M. K. Kuimova, Phys. Chem. Chem. Phys. **15**, 14986 (2013).
[33] K. Kinosita, R. Yasuda, H. Noji, S. Ishiwata, and M. Yoshida, Cell **93**, 21 (1998).
[34] T. B. Blum, A. Hahn, T. Meier, K. M. Davies, and W. Kühlbrandt, Proc. Natl. Acad. Sci. U.S.A. **116**, 4250 (2019).
[35] V. G. Almendro-Vedia, P. Natale, M. Mell, S. Bonneau, F. Monroy, F. Joubert, and I. López-Montero, Proc. Natl. Acad. Sci. U.S.A. **114**, 11291 (2017).